International Journal of Modern Physics B, Vol. 15, Nos. 6 & 7 (2001) 758–766

ORIENTATION DYNAMICS OF MAGNETORHEOLOGICAL FLUIDS SUBJECT TO ROTATING EXTERNAL FIELDS

SONIA MELLE AND MIGUEL A. RUBIO

Departamento de Física Fundamental, UNED, C/ Senda del Rey s/n, 28040 Madrid, SPAIN
E-mail: smelle@fisfun.uned.es

GERALD G. FULLER

Department of Chemical Engineering, Stanford University, Stanford, CA 94305-5025, USA
E-mail: ggf@chemeng.stanford.edu

The formation and orientation of field-induced structures in magnetorheological (MR) fluids subject to rotating magnetic fields have been studied using two optical methods: scattering dichroism and small angle light scattering (SALS). The SALS patterns show how these chain-like aggregates follow the magnetic field with the same frequency but with a retarded phase angle for all the frequencies measured. Using scattering dichroism two different behaviors for both, dichroism and phase lag, are found below or above a critical frequency. Experimental results have been reproduced by a simple model considering the torques balance on the chain-like aggregates.

1 Introduction

Magnetic fluids subjected to unidirectional external magnetic fields become optically anisotropic due to the orientation of string-like aggregates of the colloidal particles making up the suspension [1]. Indeed, optical techniques including video microscopy, light transmission and light scattering have been used to characterize the kinetics of field-induced structures formation in magnetorheological (MR) fluids [2-8]. These clusters are usually linear, rod-like chains oriented along the direction of the applied field, although for sufficiently large concentrations of dipolar particles more complex structures may arise [9,10]. Polarizable systems consisting of many elongated objects exhibit interesting dynamic behaviors when submitted to a rotating electric or magnetic field [11-13]. In this paper we report the structural evolution of MR fluids under the application of a stationary and spatially rotating magnetic field by means of scattering dichroism and Small Angle Light Scattering (SALS) techniques.

When a unidirectional magnetic field, $\vec{H}$, is applied to a suspension, the field induces a magnetic dipolar moment in the magnetic particles $\vec{m}$. For low magnetic fields, (typically less than $25KA/m$), the particles used in this study have a paramagnetic behavior, $\vec{m} = V\vec{M} = (4/3)\pi a^3 \chi \vec{H}$, being a the particle radius and χ the magnetic susceptibility of the particles. A key dimensionless parameter to characterize the formation of chains is the ratio between magnetic and thermal energy, $\lambda = (\pi \mu_0 a^3 \chi^2 H^2)/(9K_B T)$, where μ_0 is the vacuum magnetic permeability, K_B is the Boltzmann constant and T the temperature. Therefore, for the range of fields measured here $(1.2 < H(KA/m) < 25)$ we obtain $15 < \lambda < 6250$ at room temperature, so the magnetic interaction will dominate over Brownian thermal motion. Because these chains have a preferred orientation the suspension exhibits an optical anisotropy as reflected in the complex refractive index tensor, $\tilde{n}_{ij} = n'_{ij} - in''_{ij}$, being this anisotropy due to the polarization dependent scattering

from oriented aggregates. Furthermore, as the length scale of the scattering objects encountered in these measurements is comparable to the wavelength of the light, then the dichroism $\Delta n''$ (anisotropy of the imaginary part) will be larger than the birefringence $\Delta n'$ (anisotropy of the real part) [14].

Using Rayleigh-Debye theory for the scattering of light the following expression can be used to estimate the scattering dichroism in the forward direction ($\theta_{scat} = 0$) generated from a set of N chains per unit volume assuming that the chains are long circular cylinders of length L and radius R [14]:

$$\Delta n'' = \frac{2NL}{k^2}\left(\mathrm{Re}[T_2(\theta_{scat}=0)] - \mathrm{Re}[T_1(\theta_{scat}=0)]\right) \tag{1}$$

Here $k = 2\pi/\lambda$ is the wave vector and $T_i(\theta_{scat} = 0)$ is a function of $k, R,$ and the isotropic refractive indexes of solvent and particles. From (1) we deduce the dichroism is related to the number of particles forming the aggregates per unit volume given by $n_p = NL/2R$.

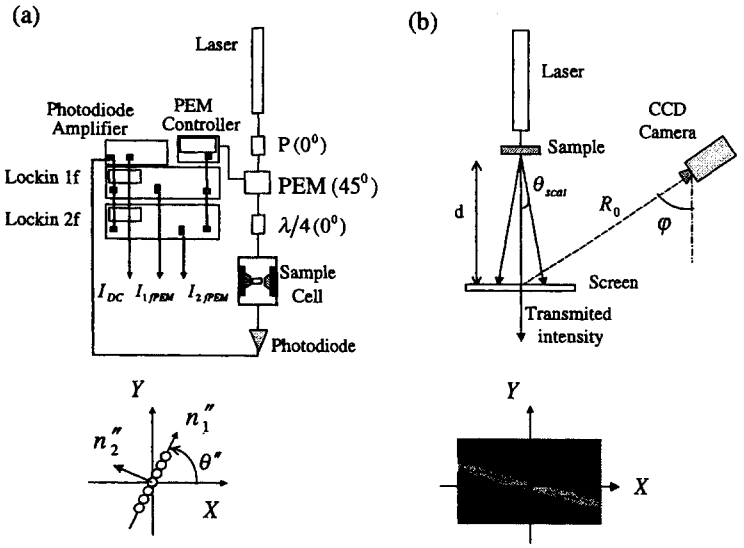

Figure Error! Unknown switch argument.. **(a)** Schematic diagram of linear dichroism optical train (up). This set up enables to simultaneously measure dichroism $\Delta n'' = n_1'' - n_2''$ and the orientation angle θ'' (down). **(b)** Schematic of SALS setup (up). Typical photograph of the SALS pattern when a unidirectional magnetic field is applied (down).

2 Experimental Methods

A schematic of the optical train used to measure linear dichroism is shown in Fig. 1 (a). With this optical train we can simultaneously calculate the dichroism $\Delta n'' = n_1'' - n_2''$ and the orientation angle θ'', where n_1'', n_2'', and θ'' are defined in Fig. 1 (a). The SALS apparatus is depicted in Fig. 1 (b). Information about the orientation of anisotropic structures can be obtained by measuring the angular variation of the scattering pattern intensity. A typical light scattering pattern obtained when a unidirectional magnetic field

is applied to the suspension is shown in Fig. 1(b). More details about the experimental setups can be found in Ref. [15].

3 Sample Cell

The fluid sample is sandwiched between two circular quartz windows held in place by a delrin attachment (external dimensions 13 x 13 x 6 mm) designed to prevent evaporation of the solvent (see Fig. 2 (b)). The inner diameter dimensions of the cell are 6.5 mm and the thickness $e = 100\mu m$ is set by a spacer. The optical measurements are taken at an area in the cell that corresponds to the diameter of the laser (3 mm). The sample is surrounded by two orthogonal pairs of magnetic coils. These coils are housed in a temperature controlled aluminum cylinder to prevent heating effects (Fig. 2 (a)). The rotating magnetic field was achieved by applying sinusoidal electric signals to the two orthogonal pairs of coils by means of two function generators referenced to one another at the phase difference of 90^0. The function generators allowed for control of both the amplitude and the frequency of the rotating magnetic field. With this setup we can achieve magnetic fields on the order of $25KA/m$ with a variation less than 3% in the vicinity of the sample. All experiments were performed at room temperature, which ranged from 20 to 22^0C.

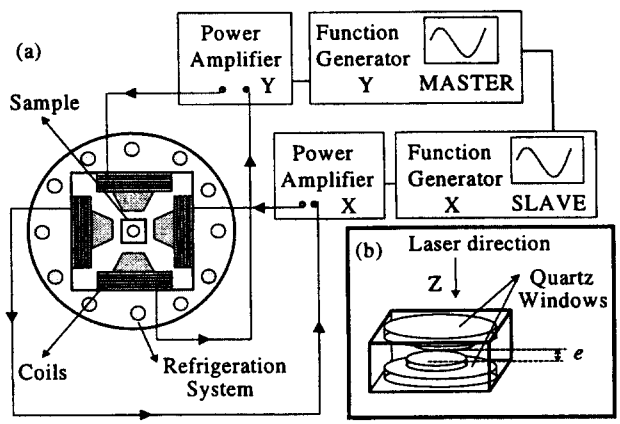

Figure 2. **(a)** Sketch of the coils system from the direction of the laser beam to produce a rotating magnetic field in the sample. **(b)** Detail of the quartz cell filled with MR fluid.

4 Magnetic Suspensions

We used a magnetic suspension manufactured by Rhône – Poulenc (M1-180/12) formed of superparamagnetic latex microspheres $(a = 0.505\mu m)$, which contain the same small ferromagnetic particles as those dispersed in a ferrofluid. These aqueous dispersions have a solids content of 10%, and a magnetite (Fe_2O_3) content of 13%. The magnetic susceptibility of the particles is $\chi = 0.96$. For our experiments we diluted this concentrated solution (M1-180/12) in glycerol to achieve a solvent volume concentration

of 82.5% glycerol with a final volume fraction of $\phi_V = 0.016$. The viscosity of this new solution without applying an external magnetic field was measured using a Rheometrics Dynamic Analyzer (RDA) to be $\eta = (0.975 \pm 0.003)$ Poises at $22^0 C$.

5 Experimental Results

As described previously, rotating magnetic fields in the plane (X,Y) perpendicular to the optical path direction (axis Z): $\vec{H}(t) = H\cos(\omega t)\vec{u}_x + Hsin(\omega t)\vec{u}_y$ were applied to the suspensions. Under these conditions, two torques act on the formed aggregates: a magnetic torque Γ_m that rotates the chain-like structures due to dipolar interaction among the particles orientated in the direction of the magnetic field, and a hydrodynamic torque Γ_h which explains the rotational friction of the structures in the suspending fluid.

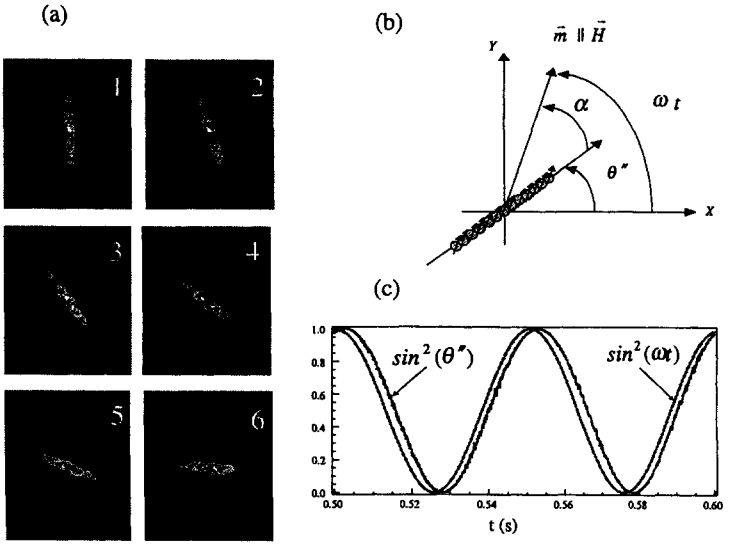

Figure 3. (a) Time evolution of scattering patterns obtained when a quarter-turn of rotating field is counterclockwise applied to the suspension. (b) Definition of the phase lag between the magnetic field and the chains. (c) Experimental signals of the temporal evolution of the magnetic field and the aggregates direction for a field strength of $H = 12.4\,KA/m$ and rotational frequency of $\omega = 2\pi \cdot 10\,Hz$.

In Fig. 3 (a) we observed the temporal evolution of SALS patterns generated by the suspension in the presence of rotating magnetic field. A qualitative interpretation of such patterns indicates that the induced structures follow the magnetic field rotating with the same frequency. In order to analyze this behavior we have simultaneously measured the time evolution of the dichroism and the orientation angle $\theta''(t)$ (defined in Fig. 3 (b)). By comparing $\theta''(t)$ with the temporal evolution of the magnetic field direction given by ωt we found, as can be observed in Fig. 3 (c), that the structures follow the magnetic field rotating with a phase lag independent on time for all frequencies measured. Therefore we define the phase lag between the field and the aggregates as $\alpha(t) = \omega t - \theta''(t)$.

In Fig. 4 (a) the dichroism generated by a suspension is plotted as a function of field strength for various frequencies of the rotating fields. All the curves show a monotonic increase in dichroism to a plateau value but with a strong dependence on the rotational frequency. This effect is shown more directly in Fig. 4 (b) where the dichroism is plotted against magnetic field frequency ($f = \omega/2\pi$) in a log-log form. As the frequency of the applied field is increased, the dichroism is strongly reduced, which indicates that hydrodynamic friction forces can overcome the dipolar magnetic forces. This plot shows clearly two distinct regions for frequencies below and above a critical frequency, f_c, near to 0.3 Hz. Below this critical frequency, the dichroism is essentially independent on frequency and therefore the aggregates size remain almost constant. However, once this frequency is surpassed, the dichroism decreases with frequency, which reveals the diminution of the aggregates size. The critical frequency separating these two regions increases with the magnitude of the applied magnetic field, as expected since the strength of the interparticle magnetic forces scales with the applied field. It is found above 1 Hz that the dichroism drops with frequency with a scaling of approximately $\Delta n'' \approx f^{-1}$.

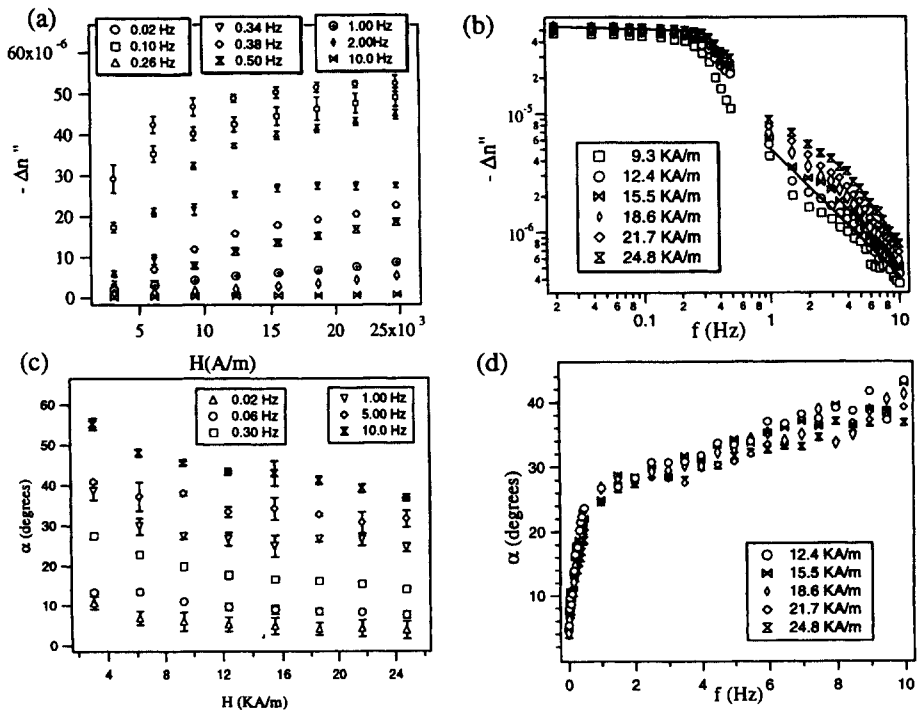

Figure 4. **(a)** Dichroism versus magnetic field intensity for frequencies ranging from 0.02 Hz to 10 Hz. **(b)** Dichroism as a function of magnetic field frequency for a range of magnetic field strength in a log-log plot. Two behaviors are found above or below a critical frequency around 0.3 Hz. **(c)** Phase lag as a function of magnetic field intensity for frequencies ranging from 0.02 Hz to 10 Hz. **(d)** Phase lag as a function of magnetic field frequency.

The phase difference α between the orientation of the chains and the magnetic field versus the field strength is plotted in Fig. 4 (c) for different rotational frequencies. We see a diminution of the phase difference with increasing magnetic field intensity as expected

because the magnetic torque increases with the magnetic field strength. Analyzing experimental data for the variation of the phase difference α with the frequency of the magnetic field (see Fig. 4 (d)), we observe that this phase difference is increasing with frequency over the whole range of frequencies. However, as we found for the dichroism results (see Fig. 4(b)), two different responses are seen depending on the frequency value. At low frequencies (below the critical frequency) the phase difference growths very quick while at high frequencies the increase of the phase difference is relatively slow.

To analyze the behavior of the phase lag we have developed a simple model considering the torque balance on the chain-like aggregates (see Appendix). A similar model has been used to explain the behavior of droplets made of a concentrated magnetic fluid [13]. With this model we deduced that in the stationary regime the phase lag follows Eq. (A6)

$$sin2\alpha \approx \frac{\pi 2^5 \eta}{\mu_0 a \chi^2} \cdot \frac{f\,L}{H^2 Ln(L/2(2a))}$$

We can rewrite this steady solution as $sin2\alpha = f / f_0$ to emphasize that two different regimens take place as we saw in the experimental results. A first regimen for low frequencies $(f < f_0)$ where the magnetic force domains and therefore the chains length remains almost constant (see Fig. 4 (b)). This implicates the phase lag increases with frequency as is deduced from Eq. (A6). Neglecting in this equation the slow logarithmic dependence, and considering that $\Delta n'' \propto L$ we find that the phase lag scaling as

$$sin2\alpha \propto \frac{f\,\Delta n''}{H^2} \tag{2}$$

To examine this scaling we plotted $(sin2\alpha)$ Vs $(\Delta n'' f)$ in Fig. 5 (a), for $f < f_c$ and for different magnetic field strengths. We find a linear behavior in agreement with our model, being the slope proportional to H^{-2} as it is shown in Fig. 5 (b) following the theoretical prediction.

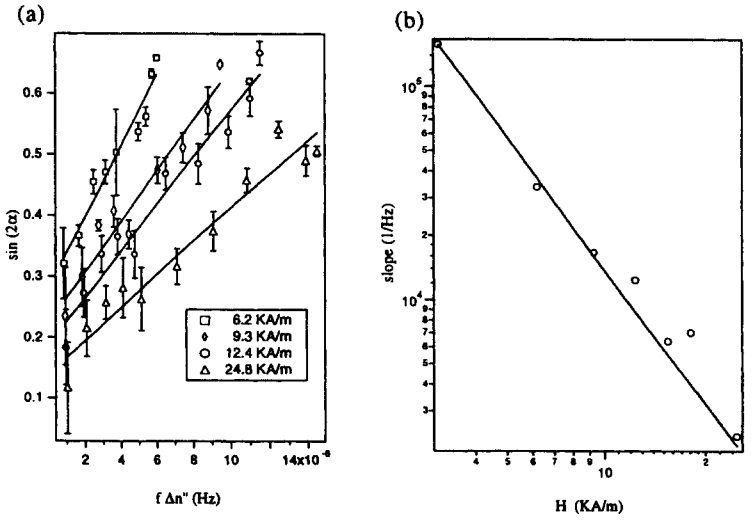

Figure 5. (a) Plot $sin(2\alpha)$ versus $(f \cdot \Delta n'')$ to test our theoretical predictions for low frequencies $(f < f_c)$ and for different magnetic field intensities. (b) Power law fit for the slope versus H in a log-log plot leading an exponent $\delta = -2.08 \pm 0.08$.

A second regime appears for high frequencies when the viscous torque becomes more important. In this regime $f \approx f_0$ so, as we observed in the experiments, the increase in the phase lag difference is relatively slow (see Fig 4 (b)) and the aggregates size is limited by

$$\frac{L}{Ln(L/2(2a))} \approx \frac{\mu_0 a \chi^2 H^2}{\pi 2^5 \eta f} \tag{3}$$

Neglecting the slow logarithmic dependence in Eq. (3), we obtain a scaling $L \propto f^{-1}$ in agreement with the dichroism dependence with frequency $\Delta n'' \propto f^{-1}$ (Fig. 4 (b)).

6 Conclusions

We have studied the structural evolution of field-induced aggregates in MR fluids when a spatially rotating magnetic field is applied by means of scattering dichroism and SALS.
The SALS patterns show how the induced chain-like structures follow the magnetic field rotating with the same frequency. In addition, using scattering dichroism we deduced the aggregates rotate at a phase angle that lags the rotating magnetic field. Two different behaviors for both, dichroism and phase lag, are found below or above a critical frequency. For low frequencies, the phase lag increases strongly while the size of the structures remains almost constant. However, for high frequencies, as the hydrodynamic forces overcome the dipolar magnetic forces, the chains break-up and the phase lag increase slower with frequency.
A torque balance model is developed to explain this behavior. The model predicts for low frequencies that this phase angle is an increasing function of the rotational frequency and a decreasing function of field strength following Eq. (2). For high frequencies the model give us a limitation in the aggregates length being $L \propto f^{-1}$. Both of these predictions are observed experimentally.

7 Acknowledgments

S.M. thanks to DGICYT (project no. PB96-0148) for financial support and Professor Fuller's group for helping in the experimental work. We gratefully acknowledge discussions with Oscar G. Calderón.

Appendix: Theoretical Model

We consider a chain formed by N_p particles ($N_p = L/2a$), with N_p odd. When a rotating magnetic field is applied (see Fig. 3(b)), this chain suffers two torques. On the one hand, a magnetic torque Γ_m because its long axis is not parallel to the single-particle dipole moments, which are aligned in the magnetic field direction, and on the other hand, a hydrodynamic torque Γ_h due to its angular velocity relative to the surrounding liquid.

To compute the magnetic torque we considered the magnetic interaction force in the direction $\vec{u}_\theta$ over the i particle and due to the rest of the particles forming the chain

$$F_i^\theta = \sum_{\substack{j=-(N_p-1)/2 \\ j\neq i}}^{(N_p-1)/2} F_{ij}^\theta = \frac{3\mu_0 m^2}{4\pi} sin[2\alpha] \cdot \sum_{\substack{j=-(N_p-1)/2 \\ j\neq i}}^{(N_p-1)/2} \frac{1}{r_{ij}^4} \tag{A1}$$

where $r_{ij} = |\vec{r}_i - \vec{r}_j| = 2a \cdot |i-j|$ is the separation between particle center i and j. The magnetic field-induced torque on an aggregate will be the sum of the torques that are exerted on each particle of the chain in the θ direction

$$\Gamma_m = 2 \cdot \sum_{i=1}^{(N_p-1)/2} F_i^\theta r_i \tag{A2}$$

The viscous torque Γ_h was calculated considering the shish-kebab model [16]

$$\Gamma_h = \zeta_r \left(\frac{d\alpha}{dt} - \omega \right), \quad \text{being} \quad \zeta_r = \frac{\pi\eta L^3}{3Ln(L/2(2a))} \tag{A3}$$

the rotational friction factor of the aggregates. Equating these two torques, the equation of motion for the rotating cylinder given by the theorem of kinetic energy is

$$I\frac{d^2\alpha}{dt^2} + \Gamma_h + \Gamma_m = 0 \tag{A4}$$

where I is the moment of inertia of the rod aggregate. We can typically neglect the inertial term because the viscous drag term dominates. Therefore, after a short transient, α reaches a steady value

$$sin2\alpha = \frac{\pi\eta f L^3}{2\mu_0 a^6 \chi^2 H^2 Ln(L/2(2a))P}, \quad \text{where} \quad P \equiv \sum_{i=1}^{(N_p-1)/2} 2\, r_i \cdot \sum_{\substack{j=-(N_p-1)/2 \\ j\neq i}}^{(N_p-1)/2} \frac{1}{r_{ij}^4} \tag{A5}$$

To simplify the calculation we consider only near neighbors interactions to compute $P \approx L^2/2(2a)^5$. Therefore Eq. (A5) remains

$$sin2\alpha \approx \frac{\pi 2^5 \eta}{\mu_0 a \chi^2} \cdot \frac{fL}{H^2 Ln(L/2(2a))} \tag{A6}$$

References

1. Scholten P.C., *IEEE Trans. Magn. MAG*-**11** (1975), pp.1400.
2. Ferminger M. and Gast A., *J. Colloid Interface Sci.* **154** (1992), pp. 522.
3. Wirtz D. and Fermigier M., *Phys. Rev. Lett.* **72** (1994), pp. 2294.
4. Lemaire E., Grasselli Y., and Bossis G., *J. Phys. II France* **2** (1992), pp. 359.
5. Hwang Y. H. and Wu X-l., *Phys. Rev. E* **49** (1994), pp. 3102.
6. Liu J. et al., *Phys. Rev. Lett.* **74** (1995), pp. 2828.
7. *Proc. 5th Int. Conf. On ER Fluids, MR Suspensions, and Associated Technology*, edited by W. A. Bullough (World Scientific, Singapore, 1996).
8. Silva A. et al., *Phys. Review E* **54** (1996), pp. 5502.
9. Wang H. et al., *Phys. Rev. Lett.* **72** .(1994), pp. 1929.
10. Jund P. et al., *Phys. Rev. Lett.* **74** (1995), pp. 3049.
11. Brochard F., *J. Phys. (France) Lett.* **35** (1974) pp. 19.
12. Lettelier D. et al., *Mater. Sci. Eng.* **C 5** (1997), pp 153.
13. Sandre O. et al., *Phys. Rev. E* **59** (1999), pp. 1736.

14. Van de Hulst H.C., *Light Scattering by Small Particles*, (Dover P., New York, 1981).
15. Fuller Gerald G., *Optical Rheometry in complex fluids*, (Oxford University Press, 1995); Fuller Gerald G., *Annu. Rev. Fluid Mech.* **22**, (1990), pp 387.
16. Doi M. and Edwards S.F., *The Theory of Polymer Dynamics*, (Clarendon Press, Oxford, 1986).